TÜBİTAK

Turk J Phys
35 (2011) , 281 – 291.
© TÜBİTAK
doi:10.3906/fiz-0911-25

A 3D model for thickness and diffusion capacitance of emitter-base junction determination in a bifacial polycrystalline solar cell under real operating condition

Senghane MBODJI[1,2], Babacar MBOW[1], Fabe Idrissa BARRO[1] and Grégoire SISSOKO[1]
[1] *Laboratory of Semiconductors and Solar Energy, Department of Physics, Faculty of Science and Technology, Cheikh Anta Diop University, Dakar-SENEGAL*
[2] *Department of Physics, University of Bambey, P.O Box 30 Bambey-SENEGAL*
e-mails: msenghane@yahoo.fr - senghanem@gmail.com

Received: 11.11.2009

Abstract

This paper aims at presenting the behaviour of the space charge region for an n^+-p-p^+ bifacial solar cell under monochromatic illumination. It also deals with mathematical relations in the describing and the use of new approach that involves both junction and back surface recombination velocities with a 3D modelling study. Based on the normalized carriers' density, versus base depth, the space-charge layer thickness ($Z_{0,u}$) is studied for various parameters such as grain size g, grain boundaries recombination velocity S_{gb}, wavelength λ and for different operating conditions. Therefore, the relationship between $Z_{0,u}$ and the diffusion capacitance C_u show that junction in the n^+-p-p^+ solar cell, with columnar grain orientation, is characterized by the plane capacitor properties.

Key Words: Grain Size, grain boundary, polycrystalline, solar cell, diffusion capacitance

1. Introduction

Characterization of the space charge layer was first developed by Shockley in 1949 [1]. As Shockley's method is accurate, for reverse and zero bias only, many methods have been presented [2–4], taking into account free carriers in the space-charge layer of the p/n junction, but also being valid for all biasing voltage.

In high-frequency C-V characteristics [5, 6] of both MIS and MOS capacitor, the Fermi potential, the substrate doping and the bulk generation lifetime in semiconductors can be determined. Exploiting the phase-sensitive LBIS analysis [7] the authors show that the phase shift introduced by the solar cell depends on the carriers' lifetime, carriers' diffusion velocity time decay and the impedance incorporated in the solar cell itself. The capacitance method is also a useful procedure for determining the diffusion length in Se-CdO photovoltaic cells [8].

Using a new approach that involves both the junction recombination velocity S_{F_u} and the back surface recombination velocity S_{b_u} in a 3D modeling a bifacial polycrystalline silicon bifacial solar cell [9], we study the space-charge layer thickness $Z_{0,u}$ and the diffusion capacitance. Within the first section, the basic theory is presented while the results related to the influence of grain size g, grain boundary recombination velocity S_{gb} and wavelength λ are presented in the second part of this paper.

2. Theory

As a n^+-p-p^+ polycrystalline solar cell is made of many small individual grains, grain boundary effects are important; an example being grain boundaries act as electron-hole traps.

With regard to physical process simulation, we can consider the fibrously oriented columnar grain as shown in Figure 1 in cross-section, Figure 2 illustrates the bifacial solar cell in a planar configuration. Considering an isolated grain in Figure 3, we made calculations in order to study the variation of the main parameters, such as grain size g, grain boundaries recombination velocity S_{gb}, wavelength λ and illumination modes.

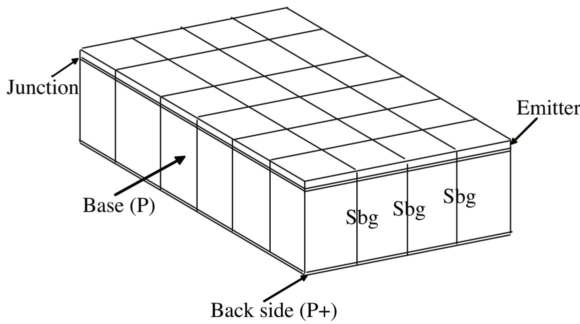

Figure 1. Fibrously oriented columnar grain.

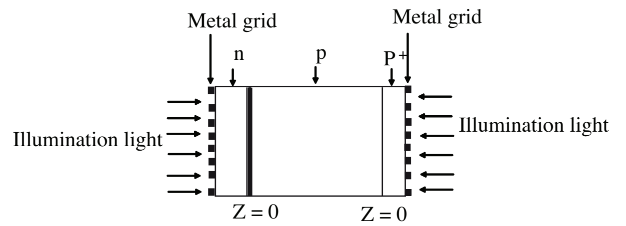

Figure 2. Bifacial solar cell.

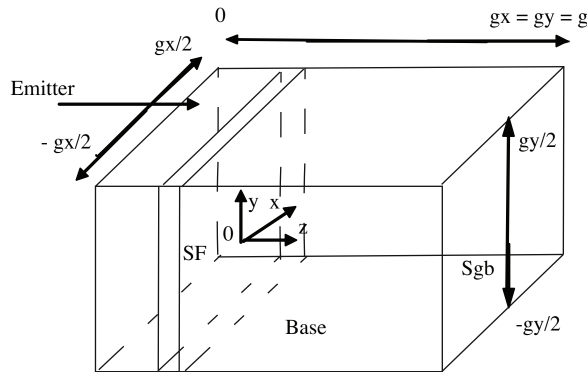

Figure 3. Schematic of an isolated grain.

Considering the emitter as a dead (non active) area, the excess minority carrier distribution in the base, seen as a greater contribution to the photo-conversion, is derived from the continuity equation [9, 10]:

$$D\left(\frac{\partial^2\delta_u(x,y,z)}{\partial^2 x}+\frac{\partial^2\delta_u(x,y,z)}{\partial^2 y}+\frac{\partial^2\delta_u(x,y,z)}{\partial^2 z}\right)-\frac{\delta_u(x,y,z)}{\tau}=-G_u(z), \quad (1)$$

where D and τ are excess minority carriers' diffusion constant and the lifetime, respectively.

Considering of these following three angles of illumination: front illumination, rear side illumination and simultaneous front and back side illumination, the electron-hole pairs generation rate is expressed as [11]

$$G_u(z) = \alpha I_0(1-R)\left(\varepsilon \cdot exp(-\alpha z) + \gamma exp(-\alpha(H-z))\right). \tag{2}$$

Table 1 shows the values of ε and γ .

Table 1. Range of ε and γ.

Illumination mode	ε	γ
Front side illumination	1	0
Rear side illumination	0	1
Simultaneous illumination	1	1

The subscript u denotes how the solar cell is illuminated: u = fr for the front side, u = re for the rear side, or u = d for double side illumination. Coefficient α denotes the absorption of light for wavelength λ; and I_0 is the incident photon flux [12].

The general solution of the continuity equation (1) is given by [9, 13]

$$\delta_u(x,y,z) = \sum_k^{\infty}\sum_j^{\infty} Z_{kj}(z)\, cos(xc_k)\, cos(yc_j). \tag{3}$$

The boundary conditions at the grain limits $\pm g_x/2$ and $\pm g_y/2$ give two transcendental equations allowing the determination of c_k and c_j [9, 10, 13, 14]. Parameter $Z_{kj}(z)$ express the z-dependence of $\delta_u(x,y,z)$.

Inserting equation (3) into equation (1), replacing the generation rate by its expression and taking into account the fact that $\cos(c_k x)$ and $\cos(c_j x)$ are orthogonal functions, we obtain a differential equation whose solution can be written as [9, 10, 13, 14]

$$Z_{kj,u}(z) = A_{kj,u} \cdot ch\left(\frac{z}{L_{kj}}\right) + B_{kj,u}\left(\frac{z}{L_{kj}}\right) - \frac{16L_{kj}^2 \cdot sin\left(\frac{gc_k}{2}\right) \cdot sin\left(\frac{gc_j}{2}\right)}{Dc_k c_j F_{kj}} \cdot G_u(z) \tag{4}$$

where

$$L_{kj} = \left(\frac{1}{L^2} + c_k^2 + c_j^2\right)^{-\frac{1}{2}} \tag{5}$$

and

$$F_{kj} = \left(g + \frac{sin\,(c_k g)}{c_k}\right) \cdot \left(g + \frac{sin\,(c_j g)}{c_j}\right). \tag{6}$$

The constants $A_{kj,u}$ and $B_{kj,u}$ in equation (4) were determined using the boundary conditions at two interfaces [9, 10, 14–16]; one interface at (a) the n^+-p boundary $z = 0$:

$$D\left.\frac{\partial \delta_u(x,y,z)}{\partial z}\right|_{z=0} = S_{F_u} \cdot \delta_u(x,y,z=0), \tag{7}$$

and (b) at the back side of the bifacial solar cell, $z = H$:

$$D\left.\frac{\partial Z_{kj}(z)}{\partial z}\right|_{z=H} = -S_{b_u}\cdot Z_{kj,u}(H). \tag{8}$$

S_{F_u} is the junction recombination velocity, written as [9, 10, 14–16] $S_{F_u} = S_{f0_u} + S_{fj}$ with S_{f0_u} being the intrinsic junction recombination velocity related to the shunt resistance due to losses occurring across the junction and S_{fj} is the imposed junction recombination velocity due external load. It defines the current flow that is the operating point of the cell. For each illumination mode, the intrinsic junction recombination velocity was calculated using the method described in [9, 10, 14–16].

S_{b_u} is the back surface recombination velocity. It quantifies the rate at which excess minority carriers are lost at the back surface of the cell [9, 10, 14–16]. The derivation of the photocurrent with respect to S_{F_u}, provides for each illumination mode the expression of S_{b_u}, as in [9, 10, 14–16].

The diffusion capacitance C_u [10, 17–19], which originates from transport of excess minority carriers in the base of the cell, can be expressed after calculation

$$C_u(z,g,S_{gb},S_{F_u},S_{b_u},\lambda) = \frac{q}{V_T}\left[\delta_u(z,g,S_{gb},S_{F_u},S_{b_u},\lambda) + m_0\right] \tag{9}$$

Here, V_T is the thermal voltage, $m_0 = \frac{n_i^2}{N_b}$ with N_b the base doping density and n_i the intrinsic carriers density.

3. Results and discussions

3.1. Normalized carriers' density versus base depth for various values of S_{F_u}

In Figures 4, 5 and 6 we show curves of normalized carriers density as a function of base depth when the solar cell is in its open circuit voltage (S_{fj} =0) or short-circuit photocurrent mode ($S_{fj} \to \infty$). Figure 4 shows the normalized carriers' density when $0 < z < 0.005$ cm for the front side illumination mode. As for the rear side and the simultaneous illumination modes, we have Figure 5 and 6 with open circuit and short-circuit operating points.

We find different characteristical regions when the solar cell is illuminated differently.

Figure 4 shows that, for the front side illumination, curves of open circuit and short-circuit exhibit a couple of regions in the base depth. The first region, close to the junction with a positive slope which increases as S_{fj} is higher and corresponds to minority carriers collection region. This space-charge region is additive (by $Z_{0,fr}$) to the initial diffusion depletion layer. Which means that space charge layer extends with increasing S_{fj} corresponding to an increase of the solar cell's photocurrent [9, 16].

Figure 5 shows that when the solar is illuminated by the rear side contrarily to the front side, the maxima points of the excess minority carriers' density are in the back side of the solar cell and are independent from the operating point. Such like the front side, we have two regions: the first region corresponds to the carriers recombined in the bulk and the ones, in low number, collected at the junction. The second region refers to carriers that are lost at the back surface of the photovoltaic solar cell. In our previous work, using this concept of the junction recombination velocity S_{F_u}, we have shown that, the rear side's transient photocurrent can be neglected when compared to photocurrents that are obtained by front side and both front and back sides [20].

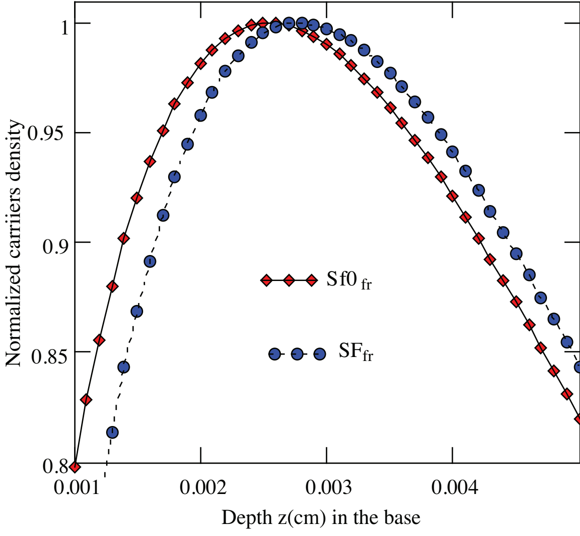

Figure 4. Normalized carrier density versus base depth when the solar cell is illuminated by front side: $g = 20\ \mu$m, $S_{gb} = 10^3$ cm. s^{-1}, $S_{f0_{fr}} = S_{b_{fr}} = 102926$ cm. s^{-1}, $H = 130\ \mu$m and $\lambda = 860$ nm.

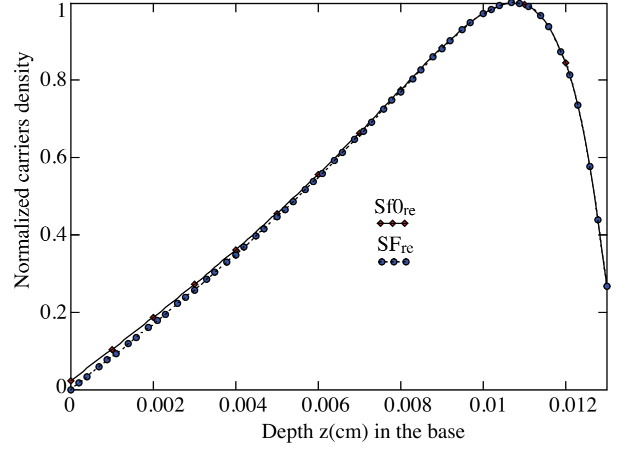

Figure 5. Normalized carrier density versus base depth for the rear side illumination mode of the solar cell: $g = 20\ \mu$m, $S_{gb} = 10^3$ cm. s^{-1}, $S_{f0_{re}} = 102923$, $S_{b_{re}} = 102925$ cm. s^{-1}, $H = 130\ \mu$m and $\lambda = 860$ nm.

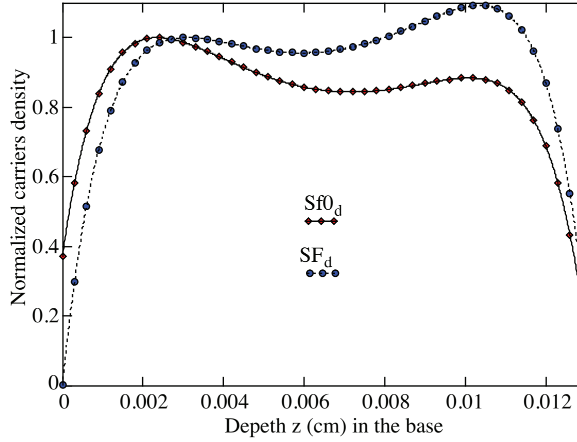

Figure 6. Normalized carrier density versus base depth when the solar cell is simultaneously illuminated both front and rear sides: $g = 20\ \mu$m, $S_{gb} = 10^3$ cm. s^{-1}, $S_{f0_d} = 66.10^3$ cm. s^{-1}, $S_{b_d} = 169204$ cm. s^{-1}, $H = 130\ \mu$m, and $\lambda = 860$ nm.

It is shown in Figure 6 that the simultaneous illumination mode gives three regions. The collection region is the first region closed to the junction, the second and third ones correspond respectively of the recombination in the bulk and the back of the solar cell.

As the junction depth varies only for front and simultaneous illumination modes (for the rear side illumination, the variation is neglected), we determine the corresponding extension region's width $Z_{0,u}$, which is linked to the Junction recombination velocity S_{F_u}. If the solar cell is operating in open circuit voltage $(S_{fj} \to 0)$, the extension region of the junction is $Z_{0,u,co}$ and if the solar cell is short-circuited $(S_{fj} \to \infty)$ we have $Z_{0,u,sc}$.The extension region's width varies from $Z_{0,u,co}$ to $Z_{0,u,sc}$ with the junction recombination velocity S_{F_u} leading of an increase of electrons which cross the junction [9, 16].

Table 2 show the diffusion capacitance C_u associated to $Z_{0,u}$ for various junction recombination velocities S_{F_u}, and shows that the diffusion capacitance decreases and the extension region width $Z_{0,u}$, increases when the junction recombination velocity increases while the voltage at the junction remains constant.

Table 2. Values of capacitance with the junction extension region width when the solar cell is illuminated at the front side (u = fr), and at both the front and rear sides (u = d).

$S_{F_u} = S_{F_{fr}}$ ($\times 10^6$ cm. s^{-1})	$S_{F_u} = S_{F_d}$ ($\times 10^6$ cm. s^{-1})	$Z_{0,fr}$ (μm)	$Z_{0,d}$ (μm)	V_{fr} (Volt)	V_d (Volt)	C_{fr} (nF. cm^{-2})	C_d (nF. cm^{-2})
1.2	-	26		0.57	-	2.6	-
-	1.066	-	33	-	0.6	-	2.500
0.3	-	25	-	0.57	-	2.7	-
-	0.166	-	30	-	0.6	-	2.700
0.2	-	24	-	0.57	-	2.8	-
-	0.076	-	27	-	0.6	-	3.015

Figures 7 and 8 show plots of inverse diffusion capacitance $C_{0,u}^{-1}$ versus space-charge layer extension $Z_{0,u}$ when the bifacial solar cell is illuminated, respectively, on its front side and, simultaneously, on the front and back sides. These Figures show that the inverse diffusion capacitance $C_{0,u}^{-1}$ versus extension thickness region $Z_{0,u}$ is a straight line. As shown by some authors [19] for the single crystal, and the given grain size, junction recombination velocity and wavelength, the diffusion capacitance C_u resulting from contribution of the free charge carriers for a solar cell in real operating point can be considered as a plane capacitor which is constructed of two identical plane electrodes situated at a variable distance from each other: the first plane electrode is fixed at $z = 0$ and the other electrode at the position $z = Z_{0,u}$ which varies with external load S_{fj}.

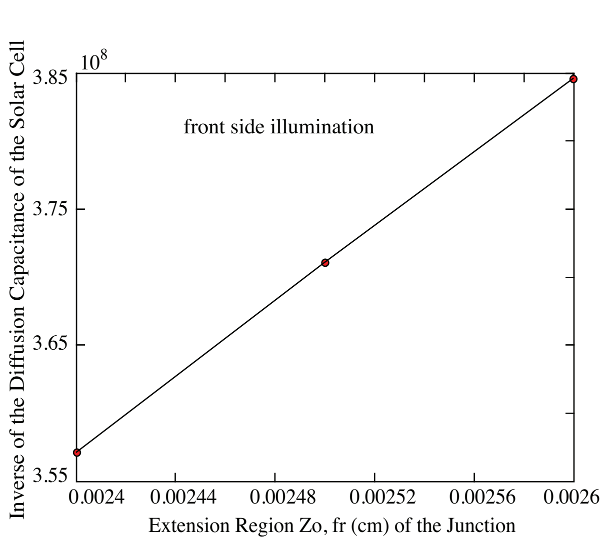

Figure 7. $C_{0,fr}^{-1}$ versus space-charge layer extension thickness ($g = 20$ μm), $S_{gb} = 10^3$ cm. s^{-1}, $S_{f0_{fr}} = S_{b_{fr}} =$ 102926 cm. s^{-1}, $H = 130\mu$m and $\lambda = 860$nm.

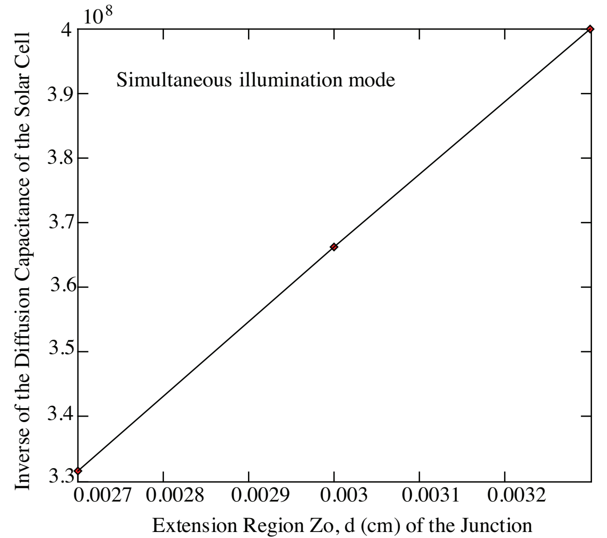

Figure 8. $C_{0,d}^{-1}$ versus space-charge layer extension thickness for $g = 20$ μm, $S_{gb} = 10^3$ cm. s^{-1}, $S_{f0_d} = 66.10^3$ cm. s^{-1}, $S_{b_d} = 169204$ cm. s^{-1}, $H = 130$ μm, and $\lambda = 860$ nm.

The diffusion capacitance C_u, which has the properties of a plan capacitor, is turned off and characterized by the extension region width $Z_{0,u,co}$ in open circuit voltage, meaning that electrons don't cross the junction.

If the junction recombination velocity S_{F_u} increases, there is a displacement of the right plane electrode of the diffusion capacitance and the electrons crossed the junction and its thickness or extension region's width reaches its limit when the solar cell is short circuited.

These results show that the junction recombination velocity S_{F_u} plays a role of a paramount importance in the explanation of losses of electrons and current flow rate in the junction as shown in [9, 16, 21] where it is noted that photocurrent and the maximum electric output provided by the solar cell increase and are calibrated with S_{fj}.

3.2. Extension region width for each grain size g, grain boundaries recombination velocity S_{gb} and wavelength λ

As we showed, that diffusion capacitance in real operating of the solar cells is a plane capacitance, we can assume that free carriers at the junction are responsible for the efficiency in semiconductors devices. As such, we can say that the diffusion capacitance C_u associated with the whole minority carriers collection layer is reduced to the Shockley's model [1, 19] when the voltage at the position $z = Z_{0,u}$ is constant.

Using one normalized carrier density versus base depth for one grain size, we determine the constant voltage $V_{u,co}(z_{0,u,co},g,S_{gb},S_{F_u},S_{b_u},\lambda)$ at $z = Z_{0,u,co}$ when the solar is open circuited.

With such a fixed voltage, we have solved equation (10) for each grain size, grain boundaries' recombination velocity and wavelength; then the corresponding extension region $Z_{0,u}$ is obtained when other parameters are fixed:

$$V_u(z,g,S_{gb},S_{F_u},S_{b_u},\lambda) = V_{u,co}(Z_{0,u,co},g,S_{gb},S_{f0_u},S_{b_u},\lambda). \tag{10}$$

The diffusion capacitance of the solar cell in open circuit voltage is then calculated using values of $Z_{0,u,co}$ through the relation [19]

$$C_{0,u} = \frac{\varepsilon S}{Z_{0,u}}, \tag{11}$$

where $S = 1\ \text{cm}^2$ and the dielectric constant $\varepsilon = \varepsilon_0\,\varepsilon_r = 12 \cdot 8.85 \cdot 10^{-14}\ F \cdot cm^{-1}$. In fact, $\varepsilon_r = 12$ is the relative dielectric constant of the semiconductor and $\varepsilon_0 = 8.85 \cdot 10^{-14}\ F \cdot cm^{-1}$ is the permittivity for the vacuum.

Results are presented below in Tables 3–5, for the front size and simultaneous front and back sides. In Figure 9 is plotted diffusion capacitance $C_{0,u,oc}^{-1}$ as a function of space-charge layer extension thickness $Z_{0,fr,oc}$ when grain size varies. We note that the inverse open circuit diffusion capacitance $C_{0,u,oc}^{-1}$ with extension region of the junction $Z_{0,u,oc}$ is a straight line, as shown by other authors [19].The junction of the solar is then considered as a plane capacitor.

Tables 3 illustrates that width of the extension region at open circuit voltage decreases with grain size, allowing a wide interval values of the thickness $Z_{0,u}$ of the diffusion capacitance and, hence, an increase of electrons crossing the junction.

Table 3. Values of characteristic parameters of the junction as g varies and the solar cell is illuminated at the front side (u = fr), and at both the front and rear sides (u = d).

g (μm)	$Z_{0,fr}$ (μm)	$Z_{0,d}$ (μm)	$E_{ZCE,u} = E_{ZCE,fr}$ (V. m^{-1})	$E_{ZCE,u} = E_{ZCE,d}$ (V. m^{-1})	$C_{0,fr}$ (nF. cm^{-2})	$C_{0,d}$ (nF. cm^{-2})
20	25.12	-	22691	-	42.27	-
23	18.56	-	30711	-	57.21	-
26	16.49	-	34566	-	64.40	-
29	15.18	-	37549	-	69.96	-
32	14.22	21.55	40084	17225	74.68	49.28
35	13.46	18.65	42347	26450	78.90	56.94
38	12.84	16.87	44392	30563	82.71	62.95
41	12.32	15.61	46266	33787	86.20	68.03
44	11.86	-	48060	-	89.54	-
47	-	14.63	-	36515	-	72.59
50	-	13.83	-	38961	-	76.78
53	-	12.57	-	41214	-	84.48
56	-	12.03	-	45346	-	88.13

Table 4. Values of characteristic parameters of the junction when Sgb varies and the solar cell is illuminated by front side and both front and rear sides.

S_{gb} (cm. s^{-1})	$Z_{0,fr}$ (μm)	$Z_{0,d}$ (μm)	$E_{ZCE,u} = E_{ZCE,fr}$ (V. m^{-1})	$E_{ZCE,u} = E_{ZCE,d}$ (V. m^{-1})	$C_{0,fr}$ (nF. cm^{-2})	C_d (nF. cm^{-2})
158	10.80	10.93	52777	51150	98.33	97.16
200	11.13	11.35	51212	50220	95.41	93.58
251	11.55	11.89	49350	47939	91.94	89.31
316	12.10	12.59	47107	45274	87.76	84.35
398	12.82	13.53	44461	42128	82.83	78.49
501	13.80	14.83	41304	38435	76.95	71.61
630	15.22	16.72	37450	34090	69.77	63.51
794	17.51	19.91	32552	28628	60.65	53.34
1000	25.42	33.09	22423	17225	41.77	32.09

Table 5. Values of characteristic parameters of the junction when λ varies and the solar cell is illuminated by front side and both front and rear side.

λ (nm)	$Z_{0,fr}$ (μm)	$Z_{0,d}$ (μm)	$E_{ZCE,u} = E_{ZCE,fr}$ (V. m^{-1})	$E_{ZCE,u} = E_{ZCE,d}$ (V. m^{-1})	$C_{0,fr}$ (nF. cm^{-2})	C_d (nF. cm^{-2})
880	22.36	-	25491	-	47.49	-
900	24.19	21.10	23563	27014	43.90	50.33
920	29.18	21.15	19533	26950	36.39	50.21
940	-	22.44	-	25410	-	47.32
960	-	25.78	-	22110	-	41.19

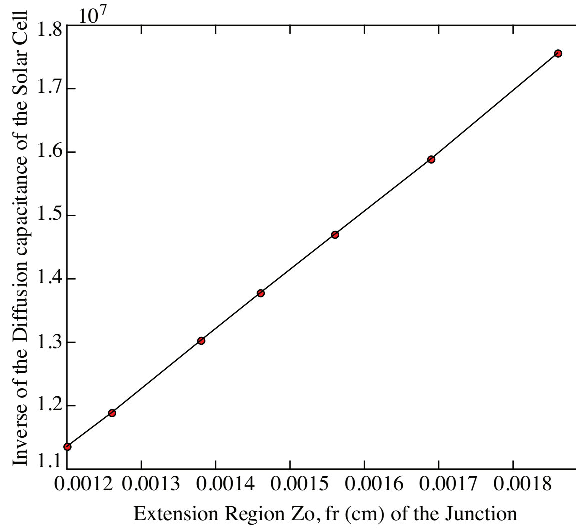

Figure 9. $C_{0,fr}^{-1}$ front side illumination mode versus space-charge layer extension thickness; here, $S_{gb} = 10^3$ cm. s^{-1}, $\lambda = 860$ nm, $D = 26$ cm^2. s^{-1}, and $H = 130$ μm.

Table 4 illustrates the increase of the extension region's width in open circuit voltage with grain boundary recombination velocity due to many recombination centers which appears when S_{gb} increases. It is known that, with the increase of these parameters, the shunt resistance, which expresses the losses at the junction, decreases corresponding to an increase of the intrinsic junction recombination velocity S_{f0_u} [22]. The series resistance expressing losses in the base material also increase, meaning that the photocurrent decreases with S_{gb} [9].

The role played by grain size and grain boundary recombination velocity is shown in [9] whereby, it is demonstrated that the number of excess minority carriers increases and decreases respectively according to the grain size g and the grain boundary recombination velocity S_{gb}; the authors in this paper [9] also proved that central areas of each grain, contrarily to the corner, are not affected by the recombination occurring at the interfaces' level. Hence, the two parameters g and S_{gb} influence the photocurrent and the photovoltage.

Table 5 shows the variation of the extension region's width in open circuit $Z_{0,u,co}$ for the wavelengths ranging from 880 to 960 nm. It is shown that $Z_{0,u,co}$ increases with wavelength due to the energy of the incoming photons; and both diffusion capacitance and excess minority carriers would decrease at the long wavelength, as we have shown in previous works [10, 17].

High values of wavelength and grain boundary recombination velocity have the same effect on $Z_{0,u,co}$, which increases towards and reaches to $Z_{0,u,sc}$, as seen in [18]. The removing of diffusion capacitance's plane electrodes is practically zero and electrons don't cross the junction.

The voltage at $Z_{0,u}$ is constant while the resulting electric field $E_{ZCE,u} = \frac{V_u}{Z_{0,u}}$, different from the intrinsic electric field E_0 of any p-n junction, increases with grain size; and when the grain boundary recombination velocity or the wavelength increases, the electric field decreases.

4. Conclusion

Using both the junction and back surface recombination velocities, the diffusion continuity equation is resolved taking into account the grain size, grain boundary recombination velocity and illumination modes.

The Junction recombination velocity S_{F_u} appears to be very important in determining the extension region width $Z_{0,u}$ of the junction which could be considered as a plane capacitor with two identical plane electrodes separated by $Z_{0,u}$. This thickness $Z_{0,u}$ increases with the junction recombination velocity S_{F_u} in correspondence to an enlargement of the space charge that leads to an increase of electrons' flow crossing the junction.

It is shown that, under open-circuit condition, if the thickness $Z_{0,u,co}$ ($\mathrm{SF}_j \rightarrow 0$) of the diffusion capacitance increases, it reaches the thickness $Z_{0,u,sc}$ in short circuit photocurrent ($\mathrm{SF}_j \rightarrow \infty$) and then the displacement of diffusion capacitance's plane electrodes is reduced and the electrons don't cross the junction. It is the case when grain boundary recombination and wavelength are high but for high grain size, there is an important gap between $Z_{0,u,co}$ and $Z_{0,u,sc}$ corresponding then to the best solar cell.

The thickness and diffusion capacitance of emitter-base junction determination can be used as characterization of solar cell efficiency, but the theoretical and stimulated values must be confirmed experimentally.

References

[1] W. Shockley, *Bell Syst.Techn.J.,* **28**, (1949), 435.

[2] J. J. Liou, F. A. Lindholm, and J. S. Park, *IEEE Trans. Electron Devices.*, **34**,(1987), 1571.

[3] B. R. Chawla, H. K. Gummel, *IEEE Transactions on. Electron Devices.*, **3, (**1971), 178.

[4] J. J. Liou, F. A. Lindholm, *J.Appl Phys.,* **3**, (1988) , 1249.

[5] K. S. Rabbani and D.R.Lamb, *Solid State Electronic.,* **24**, (1981), 661.

[6] A. Jakubowski, *Solid State Electronic.,* **24**, (1981), 985.

[7] Th.Pernau, P. Fath and E. Bucher*, Conference record of the twenty-nineth IEEE photovoltaic specialists conference*, (2002), New Orleans USA, 442.

[8] C. H. Champness Z. A. Shukri and C. H. Chan, *Can.J.Phys.,* **69**, (1991), 538.

[9] H. L. Diallo, A. S. Maiga, A. Wereme and G. Sissoko, *Eur. Phys. J. Appl. Phys.,* **42**, (2008), 203.

[10] S. Mbodji, M. Dieng, B. Mbow, F. I. Barro and G. Sissoko, Journal of Applied Science and Technology (JAST).,15, (2010), 109.

[11] G. Sissoko, A. Correa, E. Nanema, M. N. Diarra, A. L. Niaye, M. Adj, *Proceedings of the World Rrenewable Energy Congress.,* **3**, (1998), Florence, Italy, 1856–1859, Elsevier Science Ltd. 0960–1481/98 $15.00+0.00

[12] M. A. Green, and M. Keevers, *Progress in Photovoltaics.*, **3**, (1995), 189.

[13] J. Dugas, *Solar Energy Materials and Solar Cells.*, **32**, (1994), 71.

[14] M. Ndiaye, A. Diao, M. Thiame, M. M. Dione, H. LY. Diallo, M. L. Samb, I. Ly, C. Gassama, S. mbodji, F. I. Barro and G. Sissoko, *Proceedings of 25th European Photovoltaic Solar Energy Conference and Exhibition*, (2010), Valencia, Spain, 484.

[15] G. Sissoko, C. Museruka, A. Correa, I. Gaye and A. L. Ndiaye, *Proceedings of World Renewable Energy Congress*,(1996), Denver, USA, 1487.

[16] F. I. Barro, S. Mbodji, M. Ndiaye, A. S. Maiga, G. Sissoko, *Journal des Sciences.,* **8**, (2008), 37.

[17] S. Mbodji, M. Dieng , B . Mbow, F. I. Barro, G. Sissoko, *Journal des Sciences pour l'Ingénieur.,* **11,** (2009), 64.

[18] F. I. Barro, S. Mbodji, M. Ndiaye, E. Ba and G. Sissoko*, Proceedings of 23rd European Photovoltaic Solar Energy Conference and Exhibition*, (2008), Valencia, Spain, 604.

[19] G. Sissoko, B. Dieng, A. Correa, M. Adj, D. Azilino, *Proceedings of the 5th Word Renewable Energy Congress.*, **3**, (1998), Florence, Italy, 1852.

[20] S. Mbodji, A. S. Maiga, M. dieng, A. Wereme and G. Sissoko, *Global Journal of Pure and Applied Sciences.,* **15,** (2009), 125.

[21] M. L. Samb, M. Dieng, S. Mbodji, B. Mbow, N. Thiam, F. I. Barro and G. Sissoko*., Proceedings of 24th European Photovoltaic Solar Energy Conference and Exhibition*, (2009), Hamburg, Germany, 469.

[22] F. I. Barro, S. Gaye, M. Deme, H. L. Diallo, M. L. Samb, A. M. Samoura, S. Mbodji and G. Sissoko, *Proceedings of 23rd European Photovoltaic Solar Energy Conference and Exhibition*, (2008), Valencia, Spain, 612.